



HAL
open science

A new route to apply nanometric alumina coating on powders by fluidized bed chemical vapor deposition

Sana Aslam, Abderrahime Sekkat, Hugues Vergnes, Jérôme Esvan, Alessandro Pugliara, Diane Samélor, Nicolas Eshraghi, Constantin Vahlas, Jérémie Auvergniot, Brigitte Causat

► To cite this version:

Sana Aslam, Abderrahime Sekkat, Hugues Vergnes, Jérôme Esvan, Alessandro Pugliara, et al.. A new route to apply nanometric alumina coating on powders by fluidized bed chemical vapor deposition. *Chemical Engineering Journal Advances*, 2023, 16, pp.100554. 10.1016/J.CEJA.2023.100554. hal-04261424

HAL Id: hal-04261424

<https://cnrs.hal.science/hal-04261424v1>

Submitted on 2 Nov 2023

HAL is a multi-disciplinary open access archive for the deposit and dissemination of scientific research documents, whether they are published or not. The documents may come from teaching and research institutions in France or abroad, or from public or private research centers.

L'archive ouverte pluridisciplinaire **HAL**, est destinée au dépôt et à la diffusion de documents scientifiques de niveau recherche, publiés ou non, émanant des établissements d'enseignement et de recherche français ou étrangers, des laboratoires publics ou privés.



Distributed under a Creative Commons Attribution 4.0 International License



A new route to apply nanometric alumina coating on powders by fluidized bed chemical vapor deposition

Sana Aslam^{a,b}, Abderrahime Sekkat^a, Hugues Vergnes^a, Jérôme Esvan^b, Alessandro Pugliara^c, Diane Samélor^b, Nicolas Eshraghi^d, Constantin Vahlas^b, Jérémie Auvergniot^d, Brigitte Caussat^{a,*}

^a Laboratoire de Génie Chimique (LGC), Université de Toulouse CNRS, Toulouse, France

^b Centre Interuniversitaire de Recherche et d'Ingénierie des Matériaux (CIRIMAT), Université de Toulouse CNRS, Toulouse, France

^c Centre de MicroCaractérisation Raimond Castaing, Université Toulouse III Paul Sabatier, Toulouse INP, INSA Toulouse, CNRS Université de Toulouse, France

^d Corporate R&D-Umicore Belgium, Olen, Belgium

ARTICLE INFO

Keywords:

Chemical vapor deposition
Fluidized bed
Alumina thin films
Silica powder
Nanometric layers

ABSTRACT

A new route to deposit alumina nanometric thin films on powders from the single source Aluminum Tri-Isopropoxide (ATI) precursor is developed using the Fluidized Bed Chemical Vapor Deposition (FBCVD) process. For this study, an easy-to-fluidize silica powder is used, as a first step to ultimately coat cohesive oxygen sensitive powders. The FBCVD process has been studied under mild temperature conditions (400–500 °C), without any containing oxygen co-reactant. The influence of the deposition parameters (temperature, total flow rate, precursor inlet molar fraction) on the process behavior (ATI vaporization rate, fluidized bed thermal profile, deposition yield) and on the coating characteristics (composition, thickness, morphology) is analysed in details. Results show that for all conditions tested, the fluidization is maintained and the bed remains almost isothermal all along the deposition experiments, allowing for a uniform coating of the whole particles of the bed. Continuous and conformal nanometric films are obtained, mainly formed of non-carbon contaminated alumina, containing however a small amount of hydroxyl bonds that could be due to air contamination. The proof of concept of using FBCVD from ATI to produce nanometric stoichiometric alumina coatings on powders is then demonstrated, opening the way for new applications.

1. Introduction

Alumina is a highly valued ceramic material thanks to its high thermal stability, chemical inertness, hardness, high dielectric constant, and electrical insulation [1,2]. This is why it presents significant technological interest for a wide range of micro-electronic and energy storage applications [3]. It is also frequently used as a wear resistance layer and catalyst support, and as a corrosion and thermal oxidation barrier [2,4–6]. Furthermore, the application of alumina coatings on powders is a significant research area as for instance, it promotes the sintering of alumina particles for additive manufacturing of ceramic parts [7], increases the mechanical stability of nuclear fuel particles [8], and the energy density of new generations of Li-S batteries [9].

Powder coating techniques are generally of two types, (1) wet methods, which comprise sol-gel, hydrothermal, electrochemical, and

impregnation methods, (2) dry routes, which consist of pulsed laser deposition (PLD), atomic layer deposition (ALD), physical vapor deposition (PVD) and chemical vapor deposition (CVD) [10,11]. The wet methods most often necessitate the use of solvents with an additional step of calcination or separation and do not provide nanometric control of the coating thickness, contrarily to dry processes [12]. ALD and CVD are advantageous over other dry routes due to their ability to produce uniform deposits on substrates with complex geometry and high purity yield. In recent years, the use of ALD to deposit alumina coatings on powders has become popular due to its ability to form ultra-thin deposits, which is useful for energy storage applications [9]. However, it is worth studying CVD as it offers a simpler and more cost-effective process that is also capable of forming conformal coatings in the nanometer range, particularly on powders.

Fluidized bed technology has been used for many decades in

* Corresponding author.

E-mail address: brigitte.caussat@toulouse-inp.fr (B. Caussat).

<https://doi.org/10.1016/j.cej.2023.100554>

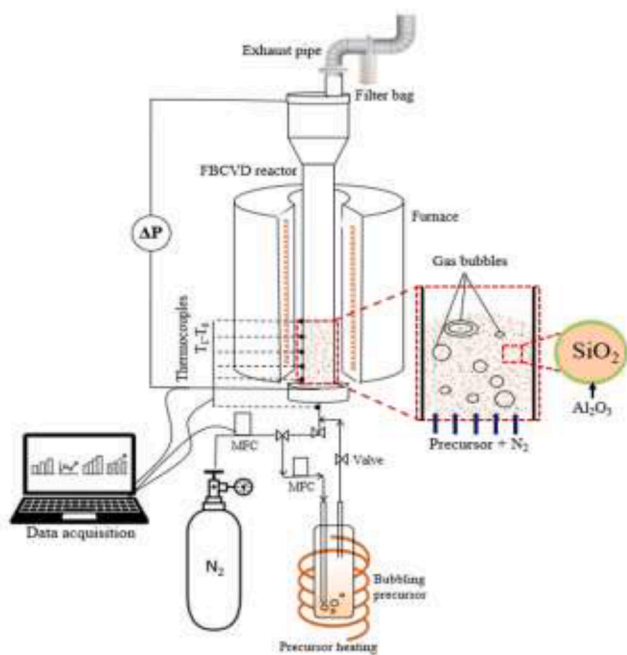


Fig. 1. Schematics of the FBCVD setup.

industries as an efficient large-scale fluid/powder contactor [13]. Fluidization is a particle suspension process that ensures good contact between powders and a fluid phase, leading to intense heat and mass transfers, uniform temperatures, high throughput, scalability, and possibility of continuous operation [14,15]. Fluidization can be combined with CVD, depending on the powder's ability to fluidize, which gives rise to the fluidized bed CVD process (FBCVD). This route offers a high conversion rate of the gaseous precursor into solid, good coating uniformity on the whole bed and on each particle of the powder, high versatility in terms of coating chemical nature, morphology and thickness, and low equipment cost [16,17].

Various CVD precursors have been tested to deposit alumina, including halides or metal organic chemicals like trimethyl aluminum (TMA), aluminum tris-isopropoxide (ATI) or aluminum acetylacetonate. Halides present the disadvantage to produce the aggressive HCl as by-product, resulting in the corrosion of the apparatus and difficulties in handling the exhaust gases. Metal organic precursors are less toxic and allow forming conformal deposits at low temperatures [18]. Among them, the alkoxide ATI presents marked advantages such as lower associated risks and costs with an ease of manipulation. It is a single source precursor avoiding any need for oxidant, which is important for powders that are sensitive to oxygen [19]. ATI has been used to deposit alumina thin films mainly under reduced pressure, but also at atmospheric pressure [19–24], conferring it a full compatibility with the FBCVD operating conditions. To the best of our knowledge, it has never been tested in a FBCVD process.

ATI is a white powder of general formula $[Al(OiPr)_3]_n$, where n depends on the physical state of the compound (solid, liquid, or gaseous), its thermal history, and storage conditions [24,23]. It can be vaporized in significant quantities thanks to its high vapor pressure [24–26]. One drawback is that it can be transformed into less volatile species on aging (limited shelf-life without protection against humidity) and on being heated [27]. It can be vaporized as a supercooled melt at 110 °C, with a carrier gas (N_2) bubbling through and it must be changed after 10–12 h of use to avoid any aging issue [24]. For Sovar [24], films processed at 5 Torr of total pressure are composed of stoichiometric Al_2O_3 when deposited above 415 °C, and of partly hydroxylated alumina when deposited between 350 and 415 °C. At 350 °C, the deposit composition is very close to $AlO(OH)$. At atmospheric pressure, pure amorphous Al_2O_3

coatings from ATI were obtained from 400 to 420 °C according to Haanappel et al. [19], and from 450 °C according to Fournier et al. [28]. These low deposition temperatures are another major reason for choosing ATI, as future coating experiments could concern thermally sensitive powders.

In the present work, the FBCVD process using ATI as a single source alumina precursor is studied to coat an easy-to-fluidize SiO_2 powder as a proof of concept, in order to find optimized process conditions to ultimately coat cohesive oxygen sensitive powders. After describing the experimental means and methods, the deposition conditions are detailed, covering the range of 400–500 °C for the average bed temperature. Their influence on the process behavior (bed thermal profile, deposition rate and yield) and on the coating thickness, composition, and morphology is thoroughly analysed.

2. Experimental

The experimental FBCVD setup is schematically presented in Fig. 1. It consists of a vertical stainless-steel reactor of 1 m height and 5 cm internal diameter. At the bottom of the column, a porous stainless-steel distributor supports the powder bed at rest and ensures a homogenous gas distribution. The external bottom part of the reactor is thermally insulated by rockwool fabrics. The top of the column is air-cooled to avoid seal degradation during coating. A filter bag is attached at the end of the exhaust pipe to collect the fine particles that could be elutriated. A two-zone external furnace heats the reactor, each zone being regulated by a PID device connected to one K-type thermocouple fixed on the outer reactor wall. Five K-type thermocouples (T1–T5) are placed into a 6 mm diameter tube along the vertical axis of the reactor to monitor the bed temperatures at various heights. One thermocouple (T6) is in contact with the bottom part of the distributor, and T6 is maintained below 150 °C to avoid any clogging of the porous plate by premature decomposition of ATI. A differential pressure sensor (LPX5480 – Druck Ltd.) is connected below the distributor and on top of the reactor to measure the total pressure drop across the bed. The whole temperatures, the bed pressure drop and the absolute pressure were registered all along the coating experiments. All CVD experiments were carried out at atmospheric pressure. An absolute pressure sensor (PR-21S, Druck Ltd.) is located below the distributor for safety reasons, in case of bed or distributor clogging. Nitrogen gas (N_2 , Air Liquide) is supplied directly to the bottom part of the reactor to fluidize the bed, and a small stream is sent to the precursor bubbler. Their flow rates are controlled by two mass flow controllers (FC-7700 type – Aera).

The ATI precursor (Sigma-Aldrich, purity $\geq 98\text{wt}\%$) is used in supercooled conditions in a glass bubbler heated by a heating mantle, as already developed by Sovar et al. [24]. This means that it is first heated at 140 °C to be melted and it is then supercooled to 110 °C and as such maintained in liquid state during the coating. The bubbler is filled with 10 g of new ATI in a glove box under argon before each experiment. Gas lines are heated at 120 °C by heating ribbons to avoid any condensation of the precursor between the bubbler and the reactor inlet.

Silica powder (Silmer Minigrain 2, purity of 99.2 wt%) with a mean diameter d_{43} of 363 μm was used as a substrate. Its diameter distribution measured by a laser granulometry setup (Malvern MS3000) is provided in Fig. S1 of Supplementary Information (SI). Its chemical composition is detailed in Table S1. The particles are non-spherical, as shown in Fig. S2. Their minimum fluidization velocity (U_{mf}) was measured under nitrogen at room temperature as equal to 0.13 $\text{m}\cdot\text{s}^{-1}$. The corresponding bed pressure drop and expansion curves are provided in Figs. S3 and S4. The elutriation of powder was estimated to be lower than 0.3 wt% per hour of fluidization at a total flow rate corresponding to 4 U_{mf} .

The powder morphology before and after coating was analysed by Field Emission Gun-Scanning Electron Microscopy (FEG-SEM) and Transmission Electron Microscopy (TEM) (imaging: Scanning TEM - High angular annular dark field (STEM-HAADF) - Chemical mapping: Scanning TEM - Energy dispersive X-ray spectroscopy (STEM-EDS)).

Table 1

Deposition conditions tested (the modified parameters in comparison with those of the nominal run S2 are highlighted in Bold).

Run	S1	S2	S3	S4	S5	S5R	S6	S7	S8
Average deposition temperature into the bed	450 °C	450 °C	450 °C	450 °C	400 °C	400 °C	500 °C	450 °C	470 °C
Fluidization ratio U/U_{mf}	4	4	4	3	4	4	4	4	4
Inlet N_2 flow rate (slm)	25	25	25	18.5	26	26	23	25	24
N_2 flow rate into the bubbler (slm)	0.6	0.6	0.3	0.6	0.6	0.6	0.6	–	0.6
Inlet molar fraction of ATI (10^{-5})	2.29	2.29	1.15	3.07	2.14	2.14	2.46	–	2.37
Deposition time (min)	165	330	330	330	330	330	330	330	330

Elemental and chemical analyses were done by Inductively Coupled Plasma-Atomic Emission Spectroscopy (ICP-AES) and X-ray photoelectron spectroscopy (XPS). Prior to FEG-SEM analyses, all the samples were submitted to ultramicrotome resin block preparation. The powder was placed in a resin, cooled down to be solidified, and then a cross-section was cut by a diamond knife. The prepared resin blocks were brought to observation by FEG-SEM in a JEOL model JSM 7100F TTLS equipped with an EDX X-Max detector from Oxford Instruments. The TEM specimens were prepared using a ThermoFisher Helios NanoLab600i dual beam Focused Ion Beam (FIB) - SEM fitted with an EasyLift micromanipulator for *in situ* lift-out. The ion (Gallium) column was operated at 30 kV for all the steps, except for final cleaning of the samples, for which tension of 5 kV was used. Transmission Electron Microscopy with a Field Emission Gun (FEG-TEM) analysis was performed using a transmission electron microscope JEOL JEM 2100 F operated at 200 kV equipped with an EDS analyser (Oxford-Instruments SDD Ultim®Max 100mm2 windowless). For ICP-AES analysis, the Al content was determined after the mineralization of the sample ($LQ = 0.005\%$ according to the validation of the analytical series), and the C content was determined by LECO elemental analyzer ($LQ = 0.005\%$). The photoelectron emission spectra were recorded using a monochromatised Al K α ($h\nu = 1486.6$ eV) source on a ThermoScientific K-Alpha system. The X-ray Spot size was about 400 μm . The Pass energy was fixed at 30 eV with a step of 0.1 eV for core levels and 160 eV for surveys (step 1 eV). The spectrometer energy calibration was done using the Au 4f $_{7/2}$ (83.9 ± 0.1 eV) and Cu 2p $_{3/2}$ (932.8 ± 0.1 eV) photoelectron lines. XPS spectra were recorded in direct mode N (Ec) and the background signal was removed using the Shirley method. The flood gun was used to neutralize charge effects on the top surface. No surface etching was applied prior to analysis.

The FBCVD operating conditions tested are listed in Table 1. Most of them were fixed according to the bibliography, in particular the average bed temperature [20,27,29] and the fluidization ratio U/U_{mf} [12,14,17,30]. The choice of the N_2 flow rate bubbling into ATI was done after preliminary tests, allowing to ascertain good bubbling conditions of N_2 into the liquid ATI at atmospheric pressure for 0.6 slm (standard liter per minute). The corresponding molar fraction of ATI is very low, which is a positive point (i) to obtain low deposition rates and thus nanometric alumina coatings and (ii) to not damage any oxygen sensitive powders due to the formation of very few amounts of water as by-product [24]. For this proof of concept study, the deposition duration was fixed such as to obtain coating thicknesses close to 50 nm, to guarantee a sufficient detection of alumina by the various characterization techniques used. For that, we performed calculations of theoretical coating thicknesses by assuming that all the ATI theoretically vaporized was fully converted into uniform coating on the bed powder. This estimation is highly approximative because (i) we assumed that the thermodynamic equilibrium is reached for the ATI vaporization in the bubbler and (ii) the ATI vapor pressure law is not precisely established in the literature. Indeed, at 110 °C, the ATI vapor pressure is 285 Pa according to Mehrotra et al. [31], 215 Pa for Bleyerveld et al. [32], and 97 Pa for Sovar [24]. The intermediate value of 215 Pa gave a theoretical maximum ATI evaporation rate close to 12 mg/min, leading to a deposition duration of 330 min. For all experiments, the initial mass of powder was equal to 294 g, corresponding to an initial fixed bed height of 15 cm. A blank

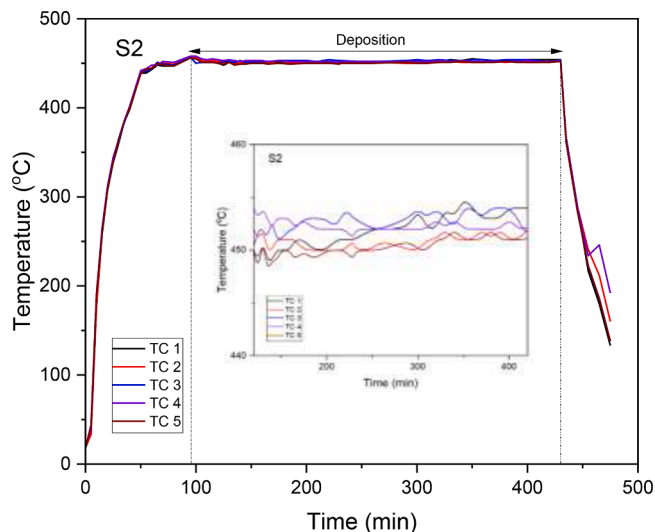


Fig. 2. Temperature profile for the experiment S2 (insert with a smaller temperature scale).

experiment (run S7) was performed in the conditions of the nominal run S2 at 450 °C, but without sending any ATI, to analyze the influence of the hydrodynamic and thermal history on the silica powder characteristics.

3. Results and discussion

3.1. Process behaviour

First, the temporal evolution of the temperature profile registered during run S2 is provided in Fig. 2 as a characteristic example of the thermal profiles measured during all runs. The thermal gradient along the bed height was lower than 6 °C during the coating, meaning that the bed remained fully fluidized. Similar values were obtained for the blank experiment S7. This good hydrodynamic behavior of the bed ensures optimal thermal and mass transfer conditions to get a uniform coating on the whole bed and around each particle. The fact that the precursor injection into the bed did not disturb the bed hydrodynamics, as it was observed for other FBCVD coatings [14], is due to the very low inlet molar fraction of ATI used. The bed pressure drop regularly increased during the reactor heating and also during the coating, due to dilatation of the steel distributor upon heating and to its partial clogging by premature ATI decomposition. A low amount of alumina was indeed deposited into the porosity of the distributor, as can be seen in Fig. S5.

The bubbler was weighed before and after each experiment, in order to measure the vaporization rate of ATI, as detailed in Table 2. For the conditions tested, between 1.5 and 3.2 g of ATI were consumed, corresponding to ATI vaporization rates between 4.5 and 10.9 mg/min. For the nominal vaporization conditions of run S2, which were used for all experiments except for run S3, 3 g on average were evaporated for each experiment, corresponding to a mean evaporation rate of 9.2 mg/min. It can be deduced from this set of experiments that the standard deviation

Table 2

Measured ATI vaporized mass from the bubbler, measured ATI evaporation rate and estimation of theoretical maximum coating thickness and deposition rate.

Run	ATI vaporized mass from the bubbler (g)	ATI evaporation rate (mg/min) (Theoretical values for 215 Pa of ATI vapor pressure at 110 °C)	Theoretical maximum coating thickness assuming all vaporized ATI is converted into alumina coating on powder (nm)	Theoretical maximum deposition rate (Å/min)
S2 – base experiment	3.6	10.9 (12.32)	142	4.3
S3 – Infl. of reducing ATI inlet	1.5	4.5 (6.16)	59	1.8
S4 – Infl. of reducing total flow rate	3.2	9.6 (12.32)	126	3.8
S5 – Infl. of temperature 400 °C	2.6	7.8 (12.32)	103	3.1
S5R – Infl. of temperature 400 °C	2.8	8.4 (12.32)	111	3.3
S6 - Infl. of temperature at 500 °C	3.2	9.6 (12.32)	126	3.8
S8 – Infl. of temperature 470 °C	2.8	8.4 (12.32)	111	3.3

Table 3

ICP-AES mass percentages of C and Al and deduced approximative alumina mass, thickness, deposition rate and yield.

Run	ICP Wt.% C	ICP net wt.%Al	Alumina mass deposited on the powder deduced from ICP (g)	Alumina thickness estimated from ICP (nm)	Deposition rate estimated from ICP (Å/min)	Deposition yield (%)
S0 (Uncoated Silica)	0.0080	0.0480*	–	–	–	–
S2 – base experiment 450 °C	0.0070	0.1120	0.62	100	3.0	70
S3 – Infl. of reducing ATI inlet	0.0100	0.0340	0.19	30	0.9	51
S4 – Infl. of reducing total flow rate	0.007	0.0620	0.34	55	1.7	44
S5 – Infl. of temperature 400 °C	0.0120	0.0920	0.51	82	2.5	80
S5R – Infl. of temperature 400 °C	0.0100	0.1020	0.56	91	2.8	82
S6 - Infl. of temperature 500 °C	0.008	0.0620	0.34	55	1.7	44
S7 – Blank experiment	0.007	0.041*	–	–	–	–
S8 – Infl. of temperature 470 °C	0.012	0.0820	0.45	73	2.2	66

* As measured values.

of ATI vaporization is 12%, which is quite low regarding the usual variations observed for such vaporization in supercooled conditions [24] and could be due mainly to temperature fluctuations of the bubbler heating mantle. By comparing the results obtained for run S3 (0.3 slm of bubbling N₂) and for the average of the other runs (0.6 slm), the ATI vaporized mass appears to be proportional to the N₂ flow rate into the bubbler. Theoretical vaporization rates were calculated from the vapor pressure of ATI at 110 °C proposed by Bleyerveld et al. [32]. For all experiments, these values at the equilibrium vary between 6.1 and 12.3 mg.min⁻¹ and are higher than the experimental ones, maybe because the residence time of N₂ in the bubbler is not high enough to fully reach equilibrium vaporization conditions, which, however, are not precisely known. From the experimental vaporization rates of ATI, theoretical maximum coating thicknesses and deposition rates (R_d) were calculated, assuming that all the vaporized ATI is converted into alumina thin film uniformly deposited on the bed particles, which were assimilated to spheres of 363 μm in diameter. Due to these assumptions, these values are highly approximate. Moreover, in these calculations, the coating on the reactor walls was neglected as the total surface area of the 294 g of silica powder (1.83 m²) is much higher than that of the reactor walls containing the silica bed (0.02 m²). For the nominal conditions of run S2, the thickness is close to 142 nm, with an average value, if considering all the experiments with similar vaporization conditions, close to 120 nm, corresponding to an average theoretical R_d of 3.6 Å/min. However, these values might be higher than the experimental ones, as there was a low amount of alumina deposited inside the porosity of the

distributor.

It was not possible to measure the deposited mass by bed weighing before/after the experiments because of (i) its too low value for the targeted thickness and (ii) the unavoidable low elutriation (~2 wt.%) occurring during the FBCVD process. ICP-AES measurements of the Al and C elements present in the powder before and after coating are provided in Table 3. The Al weight percentages for the coated samples correspond to the as measured values from which the value of the bare silica was deduced (net percentages). First, the bare silica powder (sample S0) contains a very low amount of these two elements, as mentioned in the provider data sheet (Table S1). The values obtained after the blank experiment S7 are logically of similar order of magnitude. The C weight percentage remains very low for all coated samples, inferring that for the conditions tested, the ATI decomposition was high enough to provide almost non-carbon contaminated coatings. This agrees well with the results of the literature obtained in close deposition conditions [19,24]. From the net Al content deduced from ICP, the alumina coating mass, thickness and R_d were approximately calculated, assuming another time a uniform treatment of all bed particles supposed to be perfectly spherical. A deposition yield was also estimated as the ratio between the deposition rate R_d deduced from ICP and that calculated from the ATI vaporization rate. This yield provided in Table 3 allows to evaluate the percentage of vaporized ATI effectively converted into coating on the powder.

It appears that the coating mass varies between 0.19 and 0.62 g, explaining why its direct measurement was not possible. The coating

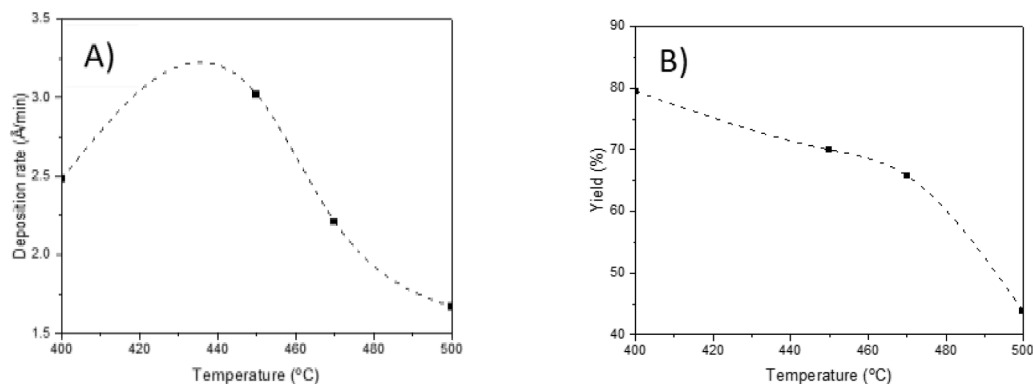


Fig. 3. Influence of the bed temperature on (A) the deposition rate and (B) the deposition yield.

thickness is comprised in the range 30 to 100 nm, in agreement with the preliminary target thickness of 50 nm for which the deposition conditions were chosen. R_d varies between 0.9 and 3 Å/min, leading to deposition yields in the 44–82% range. It is worth noting that these R_d values are two orders of magnitude lower than those obtained by Sovar [24], probably because of (i) the much lower inlet molar fractions we used (0.001–0.003% for the present study and in the range 0.2–2.45% for Sovar) and (ii) the much higher specific surface area offered by powders in comparison with conventional planar substrates. Such very low R_d are very well suited to deposit nanometric alumina coatings on cohesive powders by FBCVD because the process thus operates in a kinetically limited regime, for which the reactive species mass transfer in the gas phase is high enough to allow a uniform coating of each individual particle, even if they are embedded in agglomerates due to strong inter particles forces.

By comparing the results of runs S5 and S5R, a variation of 10% is observed on the coating mass, showing a reasonable reproducibility of the FBCVD process. From the results of runs S2 and S3, it appears that a decrease in the ATI inlet molar fraction reduces R_d , in agreement with the results of Morsinkhoff [20]. The lack of proportionality we observed (a factor two decrease of the ATI inlet molar fraction resulted in a factor three reduction of R_d) could be due to the fact that the deposition yield was lower for run S3 than for run S2, inferring that ATI was more decomposed in the porous distributor for the lowest inlet molar fraction tested. The influence of the total flow rate can be observed by comparing runs S2 and S4. By reducing the total flow rate of 25% for run S4, R_d is decreased by roughly 50% and the yield of around 40%. The lower yield could be due to the fact that when the total flow rate is decreased, the

residence time of ATI inside the distributor is higher, leading to more ATI decomposition and alumina coating of the porous distributor. This could explain the lack of proportionality between the decrease in R_d and that in total flow rate.

Concerning the key influence of the bed temperature, Fig. 3 shows that R_d increases between 400 and 450 °C, the temperature at which it reaches its maximum value (3 Å/min). Then it decreases till 500 °C to a minimum value of 1.7 Å/min. For Sovar et al. [24,29], R_d increases with temperature between 350 and 700 °C under 5 Torr of total pressure. A similar trend was observed by Morsinkhof et al. [19,20] at atmospheric pressure. The deposition yield has a monotonous decreasing evolution when the bed temperature increases, which can be explained by the fact that the amount of ATI decomposed in the distributor increases with the bed temperature, as the distributor temperature also slightly increases. Some attempts have been performed to raise of some centimetres the position of the furnace in order to limit this unwanted phenomenon, but this was not successful as the bottom part of the bed was colder than the target temperature. This is an intrinsic limitation of this FBCVD setup for the conditions tested and could certainly explain the decreasing R_d observed beyond 450 °C.

3.2. Coating characterization results

EDS mapping was recorded on all samples by FEG-SEM, after resin block preparation by ultramicrotome, as shown in Fig. S6(A). The investigation of uncoated silica (sample S0) logically showed no presence of Al, due to its low content in the bare powder (Fig. S6(B)). Sample S3 (not shown) depicted the lowest Al measurements among all the

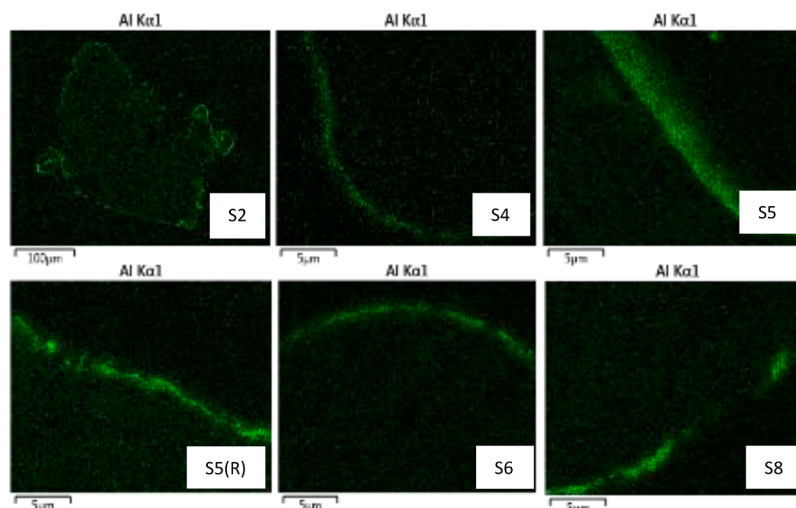


Fig. 4. Characteristic examples of aluminum EDS mapping of the samples S2, S4, S5, S5(R), S6 and S8 by FEG-SEM after resin block preparation by ultramicrotome.

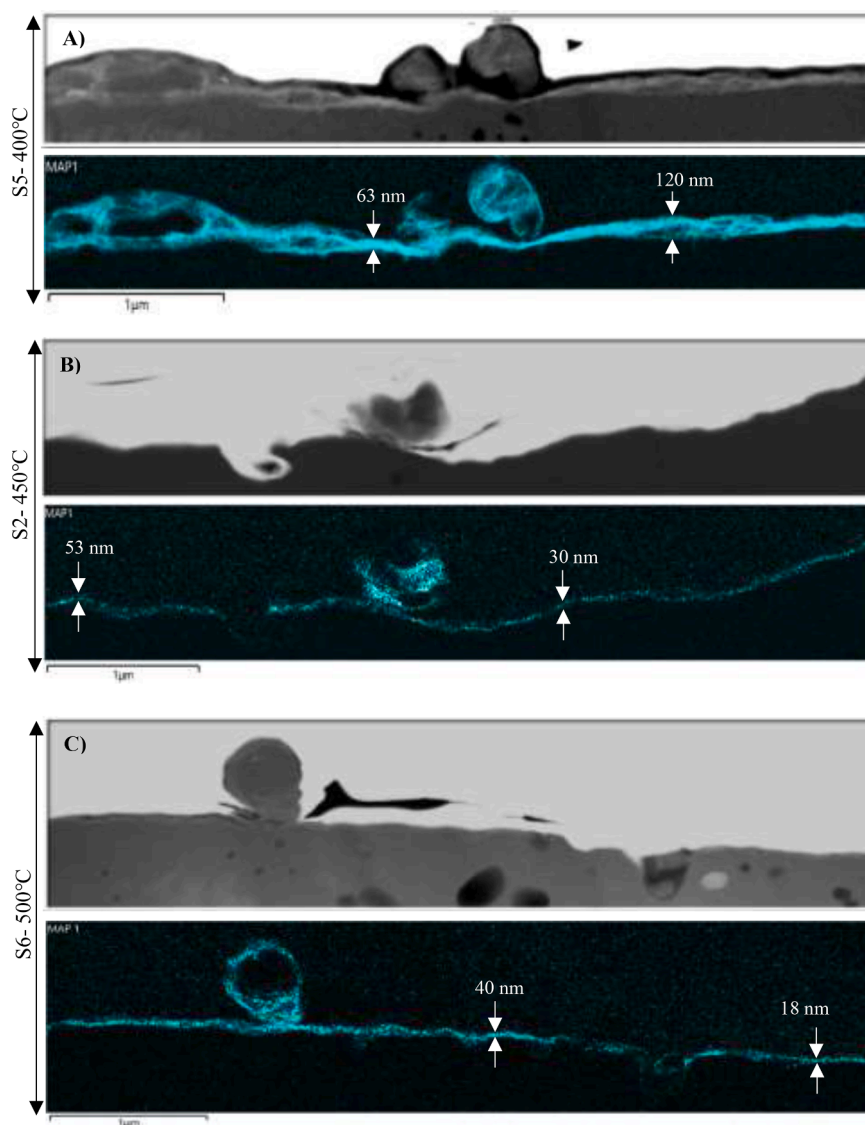


Fig. 5. STEM-HAADF images from FIB prepared lamella along with the aluminum STEM-EDS mapping for sample A) S5 (400 °C), B) S2 (450 °C), and C) S6 (500 °C).

experiments, making it difficult to identify the presence of coating on the particles. This result is coherent with the results of Table 3, as run S3 corresponds to the experiment for which the lowest Al content was measured by ICP. Fig. 4 provides characteristic examples of Al EDS mapping of all the other coated samples. After analyzing many regions of the samples, the Al coating is overall uniform and conformal. Some zones appear to be less coated, for instance for sample S8, certainly due to the very tortuous surface of the bare silica powder and to the fact that the analysed surface could not be everywhere strictly perpendicular to the electron beam. Further analyses of other particles for all these samples confirmed this outcome. Another characteristic example of results obtained is provided in Fig. S6(C) for sample S2, illustrating the conformal coating on a nodule present on the bare silica grain surface,

Table 4

Atomic percentages of Al 2p, O 1s, and Si 2p for samples S5, S2, S8 and S6 (C1s spectra included in the analysis) from XPS analyses.

Element	Atomic%			
	S5 - 400 °C	S2 - 450 °C	S8 - 470 °C	S6 - 500 °C
Al 2p	28.5	24.1	31.3	26.5
O 1s	52.3	45.3	50.9	48.6
Si 2p	7.1	6.3	6.6	2.4

which is probably not fully perpendicular to the electron beam.

TEM and EDS analyses were performed for samples S5, S2 and S6, as illustrated in Fig. 5. STEM-HAADF and STEM-EDS images confirm a conformal and continuous deposition on the silica surface of the analysed zones. It is worth noting that the measured thicknesses deduced from EDS mapping are not fully accurate due to the already explained characteristics of the bare silica powder surface, which is very tortuous and could not be everywhere perpendicular to the electron beam. Moreover, these thicknesses can hardly be compared with the values of Table 3 deduced approximately from ICP-AES, as the calculations were done by neglecting the size distribution and the irregular shape and protuberances of the silica powder. Fig. 5(A) shows for sample S5 deposited at 400 °C a continuous coating of thickness ranging from 63 to 120 nm. The EDS mapping confirms the conformal coating, even on small protuberances of the silica particles. Indeed, in certain areas, coated nodules of several hundred nanometres in size are visible, corresponding to pre-existing protuberances of the silica particles conformally coated with alumina. This result is also valid for the other samples analysed. The coating thickness for sample S2 deposited at 450 °C is within the range 30–53 nm, as measured in Fig. 5(B). Fig. 5(C) shows that for sample S6 deposited at 500 °C, a continuous coating, ranging from 18 nm to 40 nm, is present on the analysed zone and

Table 5

Atomic percentages deduced from deconvolution of Al 2p and O 1 s spectra for samples S5 and S6.

Run	Element	BE (eV)	Chemical species	Atomic%
S5 400 °C	Al 2p	74.3	Al ³⁺	100
	O 1s	531.2	O-Al	84.6
		532.6	Al-O-H	12.9
		533.8	Si-OH	2.5
S6 500 °C	Al 2p	74.5	Al ³⁺	100
	O 1s	531.2	O-Al	87.7
		532.4	Al-O-H	10
		534	Si-OH	2.3

another time covers the small protuberances present on the silica particles.

XPS was performed to unveil the chemical surface composition of the coatings deposited at different temperatures for samples S5 (400 °C), S2 (450 °C), S8 (470 °C), and S6 (500 °C), without any surface etching during the analysis. The measurements demonstrate that the Al₂O₃ signal is the most prominent as represented by the Al³⁺ extracted in all samples (Fig. S7), with an average contribution of 26.8 ± 4 at.% Al and 49.3 ± 4 at.% O across all four temperatures, as shown in Table 4. This indicates that the coated alumina films are nearly stoichiometric for all the temperatures studied, which is consistent with the results of a previous CVD study by Multone [33] and Morssinkhof [20], who used the same precursor. Furthermore, the XPS analysis of the C1s spectrum (Fig. S8) revealed a slight presence of carbon bonds, possibly originating from the carbon content in the surface of the films which was in contact with air [34]. This finding is in alignment with previous studies, which also detected a carbon contribution at the surface arising from *ex situ* contamination [33]. This is further supported by the results of the ICP analyses, which indicated the absence of carbon in the coatings. A complete XPS survey for all the samples is provided in Fig. S8 for further details.

We have performed deconvolution of the Al 2p and O 1 s spectra for the samples deposited at 400 °C (run S5) and 500 °C (run S6), as described in Table 5. Fig. 6 shows the resulting deconvolution of Al 2p and O 1 s peaks for sample S5. These results confirm the predominant contribution of the Al₂O₃ signal (Fig. 6a). Additionally, a significant proportion of 84.6 at.% at 531.2 eV, assigned to the O-Al response within the O 1 s scan, was observed for the sample S5 deposited at 400 °C (Fig. 6b). This proportion has increased to 87.7 at.% for sample S6 deposited at 500 °C. A slight contribution of Al hydroxyl (12.9 at.%) is observed at the film surface at 400 °C, which tends to decrease to 10 at.% as the deposition temperature increases to 500 °C. It could be mainly due to air contamination of the films, as found by other authors having worked on pure crystalline stoichiometric alumina in contact

with air [35]. This represents a different outcome in comparison with Fournier et al. [28] and Sovar's results [23,24,27], who obtained an Al hydroxide contribution of 25 at.% below 415 °C and a stoichiometric Al₂O₃ only above 450 °C and 415 °C respectively. This could be due to the very low inlet molar fractions we used, leading to very low deposition rates, which could favor coatings of higher purity.

4. Conclusion

Nanometric alumina layers have been deposited on easy-to-fluidize silica powders using the FBCVD process while thoroughly investigating the deposition parameters (influence of the precursor inlet molar fraction, total gas flow rate and deposition temperature). To the best of our knowledge, this is the first time that alumina coating on powders from the single source ATI precursor has been developed, opening the way to coat by alumina oxygen sensitive powders. The ATI vaporization and the FBCVD process itself demonstrated a stable and reproducible behavior. The bed remained fluidized all along the coating duration ensuring optimal thermal and mass transfers to get uniform coatings around each particle. The deposition rates were found to be two orders of magnitude lower than those of the literature studies only performed on planar substrates, due to the very low inlet molar fractions of ATI we used and to the much higher specific surface area of the pulverulent substrates. Such low deposition rates are very favourable to ensure uniform coatings around each grain of cohesive powders, which most often can be fluidized under the form of agglomerates by adding mechanical vibration to the FBCVD reactor.

For all the conditions tested, the coatings were found to be conformally deposited on the whole surface of the particles in the form of nanometric continuous layers in the range 18–120 nm, depending on the operating conditions. It is worth noting that for given processing conditions, the coating thickness can be controlled by the deposition duration. Thanks to the use of the quite reactive alkoxide ATI precursor, the deposits appeared to be non-carbon contaminated since formed of stoichiometric alumina even at 400 °C, with a slight presence of hydroxylated alumina that could be due to air contamination. The precursor utilization yield for the powder coating was up to 82%, which could be further increased by optimizing the thermal regulation of the line between the bubbler outlet and the reactor inlet and by increasing the bed height. This high yield combined with the relatively low deposition temperature and with the very low inlet molar fraction of precursor used are arguments showing the low environmental fingerprint of this FBCVD process, already known to be cost-effective and easily scalable. This study thus opens the way to conformally coat by alumina a wide range of powders for a large spectrum of applications.

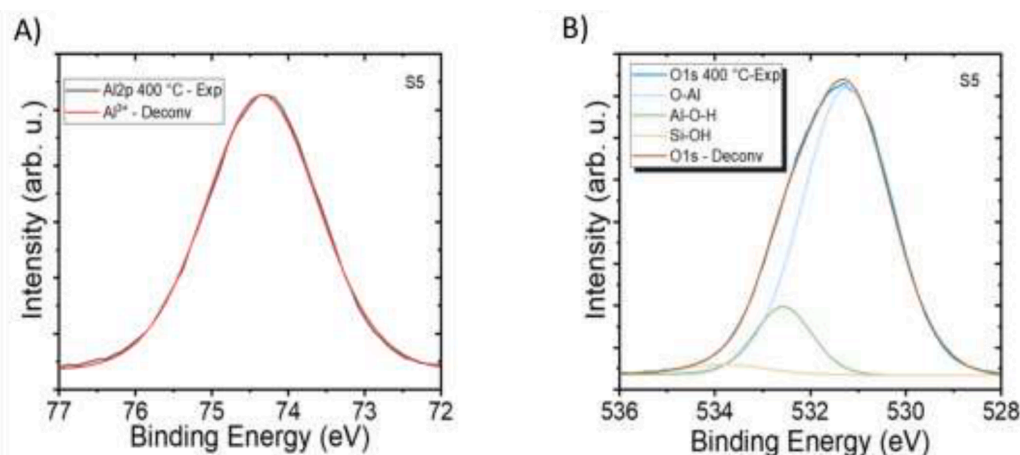


Fig. 6. Deconvolution of (A) Al 2p and (B) O 1 s XPS peaks for sample S5.

Funding information

As a part of the DESTINY European doctorate program, the authors acknowledge funding from the European Union's Horizon2020 research and innovation program under the Marie Skłodowska-Curie Actions COFUND-Grant Agreement No: 945357, and the Chairman Prof. Christian Masquelier.

Declaration of Competing Interest

The authors declare that they have no known competing financial interests or personal relationships that could have appeared to influence the work reported in this paper.

Data availability

Data will be made available on request.

Acknowledgments

As a part of the DESTINY European doctorate program, the authors acknowledge funding from the European Union's Horizon2020 research and innovation program Under the Marie Skłodowska-Curie Actions COFUND-Grant Agreement No: 945357, and the Chairman Prof. Christian Masquelier. The authors are indebted to E. Prevot from LGC for technical support, C. Josse from centre de microcaractérisation CAS-TAING for preparing the FIB lamellas, M.L. de Solan Bethmale for FEG SEM analyses into LGC and I. Fourquaux from CMEAB for preparing resin blocks by ultramicrotome for FEG-SEM analyses.

Supplementary materials

Supplementary material associated with this article can be found, in the online version, at [doi:10.1016/j.cej.2023.100554](https://doi.org/10.1016/j.cej.2023.100554).

References

- H.J.D. Souza, V. Ashith, E.D. D'Silva, Influence of preparation time on chemical bath deposited alumina (Al_2O_3) thin films, *Mater. Today Proc.* (2023), <https://doi.org/10.1016/j.matpr.2023.02.408>.
- M. Zhu, S. Achache, M. Emo, A.B. Ramírez, J.F. Pierson, F. Sanchette, Influence of the nucleation surface on the growth of epitaxial Al_2O_3 thermal CVD films deposited on cemented carbides, *Mater. Des.* 216 (2022), 110601, <https://doi.org/10.1016/j.matdes.2022.110601>.
- E. Dörr, H. Hübner, *Alumina: processing, properties, and Applications*, Springer, Berlin, Heidelberg, 1984.
- R. Usukawa, H. Katsui, K. Shimoda, S. Kondo, M. Hotta, Microstructure and integrity of multilayer ceramic coating with alumina top coat on silicon carbide by laser chemical vapor deposition, *Ceram. Int.* 49 (7) (2023) 10946–10952, <https://doi.org/10.1016/j.ceramint.2022.11.289>.
- P.L. Etchepare, D. Samelot, H. Vergnes, B. Caussat, C. Vahlas, Barrier properties and hydrothermal aging of amorphous alumina coatings applied on pharmaceutical vials, *Surf. Coat. Technol.* 425 (2021), 127711, <https://doi.org/10.1016/j.surfcoat.2021.127711>.
- A.M. Dmitrachkov, R.I. Kvon, A.V. Nartova, N-doping of alumina thin film support to improve the thermal stability of catalysts: preparation and investigation, *Appl. Surf. Sci.* 566 (2021), 150631, <https://doi.org/10.1016/j.apsusc.2021.150631>.
- W. Du, X. Ren, C. Ma, Z. Pei, Ceramic binder jetting additive manufacturing: particle coating for increasing powder sinterability and part strength, *Mater. Lett.* 234 (2019) 327–330, <https://doi.org/10.1016/j.matlet.2018.09.118>.
- S. Zhang, E. Yu, S. Gates, W.S. Cassata, J. Makel, A.M. Thron, C. Bartel, A. W. Weimer, R. Faller, P. Stroeve, Helium interactions with alumina formed by atomic layer deposition show potential for mitigating problems with excess helium in spent nuclear fuel, *J. Nucl. Mater.* 499 (2018) 301–311, <https://doi.org/10.1016/j.jnucmat.2017.11.029>.
- E. Azaceta, S. García, O. Leonet, M. Beltrán, I. Gómez, A. Chuvilin, A. Mainar, J. Blazquez, M. Knez, Particle atomic layer deposition as an effective way to enhance Li-S battery energy density, *Mater. Today Energy* 18 (2020), 100567, <https://doi.org/10.1016/j.mtener.2020.100567>.
- Q. Kuang, S.F. Li, Z.X. Xie, S.C. Lin, X.H. Zhang, S.Y. Xie, R.B. Huang, L.S. Zheng, Controllable fabrication of SnO_2 -coated multiwalled carbon nanotubes by chemical vapor deposition, *Carbon* 44 (7) (2006) 1166–1172, <https://doi.org/10.1016/j.carbon.2005.11.001>. N.Y.
- A. Goulas, J.R. van Ommen, Scalable production of nanostructured particles using atomic layer deposition, *Kona Powder Part. J.* 31 (2014) 234–246, <https://doi.org/10.14356/kona.2014013>.
- P. Rodriguez, B. Caussat, X. Iltis, C. Ablitzer, M. Brothier, Alumina coatings on silica powders by fluidized bed chemical vapor deposition from aluminium acetylacetonate, *Chem. Eng. J.* 211 (2012) 68–76, <https://doi.org/10.1016/j.cej.2012.09.048>.
- S. Balaji, J. Du, C. White, B.E. Ydstie, Multi-scale modeling and control of fluidized beds for the production of solar grade silicon, *Powder Technol.* 199 (1) (2010) 23–31, <https://doi.org/10.1016/j.powtec.2009.04.022>.
- F. Vanni, M. Montaigu, B. Caussat, C. Ablitzer, X. Iltis, M. Brothier, Fluidized-bed chemical vapor deposition of silicon on very dense tungsten powder, *Chem. Eng. Technol.* 38 (7) (2015) 1254–1260, <https://doi.org/10.1002/ceat.201400350>.
- S.S. Liu, W.D. Xiao, Numerical simulations of particle growth in a silicon-CVD fluidized bed reactor via a CFD-PBM coupled model, *Chem. Eng. Sci.* 111 (2014) 112–125, <https://doi.org/10.1016/j.ces.2014.02.021>.
- C. Vahlas, B. Caussat, P. Serp, G.N. Angelopoulos, Principles and applications of CVD powder technology, *Mater. Sci. Eng. R Rep.* 53 (1–2) (2006) 1–72, <https://doi.org/10.1016/j.mser.2006.05.001>.
- P. Lassègue, L. Noé, M. Monthieux, B. Caussat, Fluidized bed chemical vapor deposition of copper nanoparticles on multi-walled carbon nanotubes, *Surf. Coat. Technol.* 331 (2017) 129–136, <https://doi.org/10.1016/j.surfcoat.2017.10.046>.
- C. Pflitsch, A. Muhsin, U. Bergmann, B. Atakan, Growth of thin aluminium oxide films on stainless steel by MOCVD at ambient pressure and by using a hot-wall CVD-setup, *Surf. Coat. Technol.* 201 (1–2) (2006) 73–81, <https://doi.org/10.1016/j.surfcoat.2005.10.036>.
- V. Haanappel, H. Van Corbach, R. Hofman, R. Morssinkhof, T. Fransen, P. Gellings, Formation of thin oxide films by metal-organic chemical vapour deposition, *High Temp. Mater. Process.* 15 (4) (1996) 245–262, <https://doi.org/10.1515/HTMP.1996.15.4.245> (London).
- R.W.J. Morssinkhof, The deposition of thin alumina films on steels by MOCVD: synthesis, characterization and protective properties against high-temperature corrosion. Phd thesis, University of Twente, Netherlands, 1991.
- R.W.J. Morssinkhof, T. Fransen, J. Westheim, P. Gellings, Thin alumina and silica films by chemical vapor deposition (CVD), *Mater. Manuf. Process* 8 (3) (1993) 315–329, <https://doi.org/10.1080/10426919308934836>.
- R.W.J. Morssinkhof, T. Fransen, M. Heusinkveld, P. Gellings, Mechanistic aspects of the deposition of thin alumina films deposited by MOCVD, in: *Proceedings of the MRS Online Library (OPL)* 168, 1989, p. 125, <https://doi.org/10.1557/PROC-168-125>.
- M.M. Sovar, D. Samélor, A. Gleizes, C. Vahlas, Aluminium tri-iso-propoxide: shelf life, transport properties, and decomposition kinetics for the low temperature processing of aluminium oxide-based coatings, *Surf. Coat. Technol.* 201 (22–23) (2007) 9159–9162, <https://doi.org/10.1016/j.surfcoat.2007.04.063>.
- M.M. Sovar, Du tri-isopropoxyde aux oxydes d'aluminium par dépôt chimique en phase vapeur: procédé, composition et propriétés des revêtements obtenus. Phd thesis, INP Toulouse, France, 2006. <http://ethesis.inp-toulouse.fr/archive/00000392/>.
- K. Mazdiyasi, C. Lynch, J. Smith, The preparation and some properties of yttrium, dysprosium, and ytterbium alkoxides, *Inorg. Chem.* 5 (3) (1966) 342–346, <https://doi.org/10.1021/ic50037a003>.
- D. Bradley, A structural theory for metal alkoxide polymers, *Nature* 182 (4644) (1958) 1211–1214, <https://doi.org/10.1038/1821211b0>.
- A.N. Gleizes, C. Vahlas, M.M. Sovar, D. Samélor, M.C. Lafont, CVD-fabricated aluminium oxide coatings from aluminium tri-iso-propoxide: correlation between processing conditions and composition, *Chem. Vap. Depos.* 13 (1) (2007) 23–29, <https://doi.org/10.1002/cvde.200606532>.
- J. Fournier, W. DeSisto, R. Brusasco, M. Sosnowski, R. Kershaw, J. Baglio, K. Dwight, A. Wold, Preparation and characterization of thin films of alumina by metal-organic chemical vapor deposition, *Mater. Res. Bull.* 23 (1) (1988) 31–36, [https://doi.org/10.1016/0025-5408\(88\)90221-8](https://doi.org/10.1016/0025-5408(88)90221-8).
- M.M. Sovar, D. Samélor, A. Gleizes, P. Alphonse, S. Perisanu, C. Vahlas, Protective alumina coatings by low temperature metalorganic chemical vapour deposition, *Adv. Mater. Res.* 23 (2007) 245–248, <https://doi.org/10.4028/www.scientific.net/AMR.23.245>.
- P. Lassègue, N. Coppey, L. Noé, M. Monthieux, B. Caussat, Decoration of carbon nanotubes by semiconducting or metallic nanoparticles using fluidized bed chemical vapour deposition, *KONA Powder Part. J.* 33 (2016) 322–332, <https://doi.org/10.14356/kona.2016018>.
- R. Mehrotra, A. Rai, Aluminium alkoxides, β -diketonates and carboxylates, *Polyhedron* 10 (17) (1991) 1967–1994, [https://doi.org/10.1016/S0277-5387\(00\)86025-8](https://doi.org/10.1016/S0277-5387(00)86025-8).
- R. Bleyerveld, W. Fieggen, H. Gerding, Structure and physical properties of aluminium alkoxides. Part IV: vapour pressures of aluminium isopropoxide, *Recl. Trav. Chim. Pays Bas* 91 (4) (1972) 477–482, <https://doi.org/10.1002/recl.19720910410>.
- X. Multone, High Vacuum Chemical Vapor Deposition (HV-CVD) of Alumina Thin Films, Phd thesis, EPFL, Swiss, 2009, <https://doi.org/10.5075/epfl-thesis-4485>.
- T. Tuguhuro, N. Kataoka, H. Tanaka, K. Kinoshita, S. Kishida, XPS study from a clean surface of Al_2O_3 single crystals, *Procedia Eng.* 216 (2017) 175–181, <https://doi.org/10.1016/j.proeng.2018.02.081>.
- P.K. Nayak, J.A. Caraveo-Frescas, Z. Wang, M.N. Hedhili, Q. Wang, H.N. Alshareef, Thin film complementary metal oxide semiconductor (CMOS) device using a single-step deposition of the channel layer, *Sci. Rep.* 4 (1) (2014) 4672, <https://doi.org/10.1038/srep04672>.